Cell-Level PV Module Temperature Estimation Method

Haining Wang, Yuming Chen, Tao Fan, Changzhi Zhang, Weichen Ni, Jian Xu, and Jian Zhang

***Abstract*—In this article, we analyze the characteristics of current–voltage (I–V) curves of photovoltaic (PV) modules in the hotspot state, determine characteristic quantities for identifying specific hotspot state information in the utilized module, and establish an inverse solution model for estimating the normal module temperature according to the electrical characteristics of the module. We combine this inverse solution model with a heat balance model to estimate the temperature of a faulty cell and obtain the overall temperature distribution in the module. Finally, infrared data on hotspot modules collected at a power plant in Hubei are used to verify the feasibility and accuracy of the temperature estimation algorithm. The experimental results show that the proposed PV cell temperature estimation method can determine the temperature distributions in different module areas and provide technical support for module-associated fire warnings.**

***Index Terms*—Current–voltage characteristics, hotspot, photovoltaic systems, PV cell temperature estimation.**

I. Introduction

In RECENT years, the installed capacities of domestic and foreign photovoltaic (PV) power plants have increased rapidly. According to the International Energy Agency, the total installed capacity of global PV power plants is predicted to exceed 1700 GW by 2030 [1], and PV modules are expected to be used by hundreds of millions of people. However, the operation of PV modules often produces hotspot phenomena, causing sharp increases in local module temperatures and potentially inducing fires. To ensure the safety and stability of PV systems, the temperatures of PV modules should be monitored.

Manuscript received 13 June 2022; revised 22 July 2022; accepted 22 August 2022. Date of publication 8 September 2022; date of current version 28 November 2022. This work was supported in part by the National Key R&D Program of China under Award 2018YFB1500800, in part by the Technology Project of State Grid Co., LTD under Award SGTJDK00DYJS2000148, in part by the Basic Operating Expenses of Central Scientific Research under Award PA2020GDGP0053, and in part by the 111 Project under Award BP0719039. *(Corresponding authors: Yuming Chen; Jian Xu.)*

Haining Wang, Yuming Chen, and Jian Zhang are with the Engineering Research Center of Ministry of Education for Photovoltaic System, Hefei University of Technology, Hefei 230009, China (e-mail: ahwhn@126.com; 1623433329@qq.com; zhangjian_pv@sohu.com).

Tao Fan is with the State Grid Corporation of China, Beijing 100031, China (e-mail: fan-tao@sgcc.com.cn).

Changzhi Zhang and Weichen Ni are with the State Grid Tianjin Electric Power Research Institute, Tianjin 300220, China (e-mail: 13920889624@163.com; 13821175295@163.com).

Jian Xu is with the Hefei University of Technology, Hefei 230026, China (e-mail: xujian970630@163.com).

Color versions of one or more figures in this article are available at https://doi.org/10.1109/JPHOTOV.2022.3203292.

Digital Object Identifier 10.1109/JPHOTOV.2022.3203292

In previous studies [2], [3], module temperature estimations and fault identifications were carried out by acquiring infrared images of arrays. However, a power plant with a capacity of only 200 kW uses more than 800 modules and has a distribution area of several thousand square meters, and the cost of acquiring images with high identification accuracy was extremely large. In the literature [4], an equation for obtaining the current–voltage (I–V) characteristics of a PV module using the Lambert W transcendence function was established, providing a theoretical method for determining the PV module temperature based on the output characteristics of the PV module. However, the Lambert W transcendence function is difficult to solve, and some complications arise when temperature estimates are determined with this function. Some scholars have analyzed temperature variations in PV modules from a thermodynamic perspective; for example, the Sandia model [5] estimates the module temperature using the backsheet temperatures of the module and ambient irradiation, and the nominal operating cell temperature (NOCT) model [6] estimates the module temperature based on the ambient temperature. However, the estimation accuracies of these models are poor. Thus, another study [7] divided the modules into glass cover layers, cell layers, and backsheet layers and developed separate temperature estimation models to improve the overall estimation accuracy. However, these calculations use the backplane temperature of the module as an input parameter, and this parameter is difficult to acquire in actual power plants. Thus, in the literature [8], [9], extensive experimental data have been used to establish mathematical models that connect the module temperature to the wind speed, ambient temperature, and irradiance using backpropagation (BP) neural networks. However, the estimation accuracies of these models are limited by the training process, and the generalizability of these models to different types of modules and power plants in various regions is poor. In the literature [10], [11], the relationship between module irradiation and temperature has been modeled using the maximum power and *I–V* curve parameters of the module. These studies considered the entire module in analyses and used single temperature values to characterize the temperature state of the entire module. However, in practice, the temperature anomalies in PV modules typically appear as high temperatures at localized positions in the module. The temperature differences among different locations in a PV module with a hotspot can be on the order of hundreds of degrees Celsius [12], inducing severe fire hazards. Thus, the use of only one temperature value cannot reasonably describe the temperature state of a PV module.

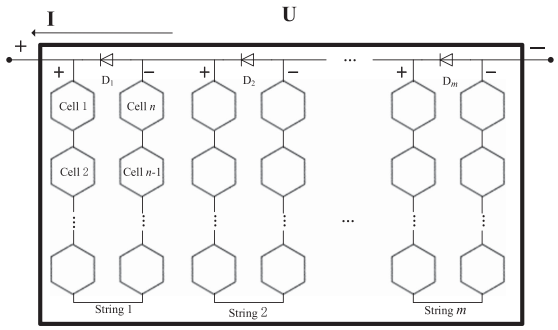

Fig. 1. Schematic diagram of the internal structure of a general PV module.

In summary, the existing methods used to estimate PV module temperatures have high hardware costs, difficult model solutions, and unreasonable temperature descriptions. To address these issues, we investigate the *I–V* characteristics of PV modules. First, based on the relevant literature, we determine the feasibility of analyzing the PV module hotspot state based on the PV module characteristics and provide characteristic parameters for identifying hotspots. Second, we establish an inverse solution model to estimate the normal PV module temperature based on the electrical characteristics of the PV module. A physical model was designed to estimate the temperature of a faulty PV cell based on the power of the heat balance, and the temperatures of normal and faulty PV cells were estimated. Finally, the proposed algorithm was verified with infrared data of a hotspot PV module collected at a power station in Badong, Hubei, confirming the accuracy and feasibility of the temperature estimation method.

The contributions of this article can be summarized as follows. First, the proposed method has lower hardware costs than previous methods, as the input parameters for the temperature estimation do not depend on the type of module temperature data and depend only on the environmental and module-related electrical data available in conventional power plant monitoring systems, thus greatly reducing hardware costs. Second, the proposed method allows more refined analyses of targets, as the temperature estimation is performed at the cell level, addressing the issue of inadequate module-level temperature descriptions. Finally, the proposed method exhibits better real-time performance than unmanned aerial vehicles (UAVs) that regularly collect infrared images. This article proposes a feasible method for monitoring module temperatures in PV power plants in real time, thus providing technical support for fire warnings in power plant systems.

II. Hotspot Identification

A PV module in a power station can be subdivided into cells and cell strings. Fig. 1 shows that PV modules are composed of several PV cells connected in series and several diodes connected in parallel. These diodes conduct if the cell fails to bypass part of the cell. We denote the group of cells controlled by the same bypassing diode as a string. In Fig. 1, because cells $1\sim n$ are controlled by diode D_1, cells $1\sim n$ are called a string. Fig. 1 shows a PV module with m strings, where each string contains n cells, resulting in a total of $N = m * n$ cells arranged in a series–parallel structure.

TABLE I
Characteristics of PV Module *I–V* Curves in Modules With Different Faults

Fault type	I-V curve characteristics
Diode short circuit	Proportional drop in U_{oc}
Proportional-integral-derivative	Open-circuit voltage reduction
Shadow	Inflection point and flat stages
Hotspot	Inflection point and inclined stages
Broken glass	Inflection points exist, and steps are characterized by convex functions

Additionally, each string is equipped with a bypass diode. To accurately analyze the module temperature, the operating state of the module, i.e., whether a hotspot exists, the number of strings affected by the hotspot fault, and the number of cell units in the strings, must be determined based on the module characteristics. This determination has been studied in previous literature [13] on PV modules with optimizers using *I–V* curve-scanning functions. By obtaining the *I–V* curves of modules in various fault states, the characteristic performance of module *I–V* curves in common fault states can be summarized, as shown in Table I.

Under maximum power point tracker (MPPT) control, operating PV modules exhibit small fluctuations around the current maximum operating point; however, the characteristics of hotspot failure are reflected as multiple steps and fold changes in the *I–V* curve. Therefore, the specific hotspot status within the PV module is difficult to determine based on only the MPPT control data of the operating PV module. Thus, in this article, we identify hotspots directly based on the morphological characteristics of the PV module *I–V* curve.

As shown in Table I, when at least one hotspot cell exists in a PV module, the *I–V* curve exhibits an inflection point and a sloping stage, while the *I–V* curves of normal modules with no hotspots do not exhibit these characteristics. These characteristics in the *I–V* curve scan results can be used to qualitatively determine whether a hotspot fault exists in a module. In addition, previous studies [14] have shown that when a module has multiple string hotspots or multiple cell hotspots in a single string, the module I–V curve exhibits different characteristics, as shown in Fig. 2.

Fig. 2(a) shows the *I–V* curve of a module with three strings, where hotspot cells exist in two of the strings. If the hotspot degrees of the two cells are exactly the same, their antiparallel diodes conduct simultaneously as the module current increases, and the faulty string is bypassed. The *I–V* curve displays an inflection point and a sloping stage, and the voltage decreases to approximately two-third of the open module circuit voltage, while the module short-circuit current shows no change, as expressed in curve 1. If the hotspot degrees of the two cells are inconsistent, the antiparallel diode of the string containing the single cell with the largest mismatch degree conducts first as the PV module current increases, while the diode in the weaker hotspot string conducts later. At this point, the *I–V* curve displays an inflection point and two sloping stages, while the short-circuit current remains constant, as shown in curve 2. If a hotspot cell exists in all three cell strings in the PV module or if multiple

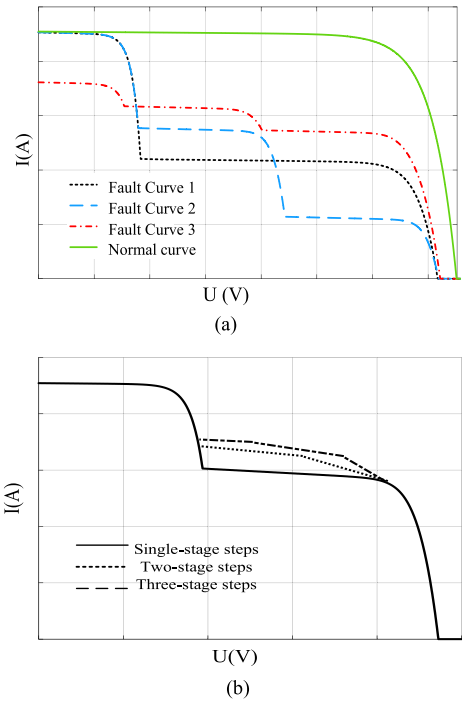

Fig. 2. *I–V* curve characteristics of hotspot assemblages in PV modules. (a) Multiple strings with a single hotspot cell. (b) Multiple hotspot cells in a single string.

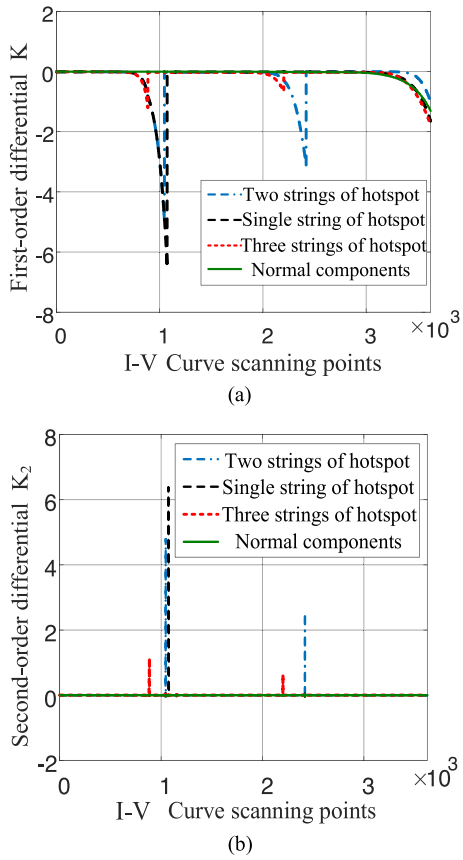

Fig. 3. Differential images of PV module *I–V* curves for modules with multiple strings containing single hotspot cells. (a) First-order difference image. (b) Second-order difference image.

hotspot cells exist within a single string in the module, the *I–V* curve displays an inflection point and two stages, but the short-circuit current is reduced, as shown in curve 3. As shown in Fig. 2(b), if multiple hotspot cells are located within a single string in a PV module, the *I–V* curve displays a folded segment at each stage due to the superposition of the reverse biased characteristics of the cells, where the number of segments is equal to the number of hotspot cells.

In summary, the morphological characteristics of PV module *I–V* curves in various fault states can be used to determine the numbers and distributions of hotspot strings and single cells in the modules. A simulation model can be developed for the four single-cell hotspot conditions shown in Fig. 2(a). Because the probability of two strings containing hotspots of the same degree is low in practice, this situation was replaced with the most common scenario, namely, a single-string hotspot in a module. Then, the module voltage in the model was increased uniformly while the module current was collected, and the ratio of the first-order difference in the current scan value to the first-order difference in the voltage scan value, K, was calculated. Then, the difference in K, namely, the second-order difference K_2, was determined, and the results are shown in Fig. 3.

Similarly, consider the case of a string with multiple hotspot cells. First, consider a PV module that contains two strings with hotspots of different degrees. If the strings contain one or two cell units with different hotspot degrees, their *I–V* curves can be scanned, and the same data processing as described above can be performed. The results of this scenario are shown in Fig. 4.

Figs. 3(a) and 4(a) show that as long as the module contains a hotspot fault, the first-order difference curve corresponding to

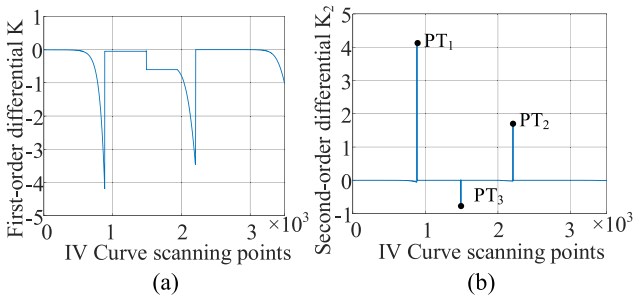

Fig. 4. Differential images of PV module *I–V* curves obtained when several strings each contain multiple hotspot cells. (a) First-order differential. (b) Second-order differential.

the *I–V* scan curve of the module has a nonconducting point. Figs. 3(b) and 4(b) show that when the short-circuit current remains approximately constant, the number of outliers with positive values on the second-order difference curve corresponding to the *I–V* scan curve is equal to the number of strings with a hotspot fault. However, when the short-circuit current is significantly reduced, all the strings contain hotspot faults. Furthermore, the number of negative outliers between the two positive outliers on the second-order difference curve corresponding to the *I–V* scan curve is increased by one and is thus equal to the total number of hotspot cells in the string.

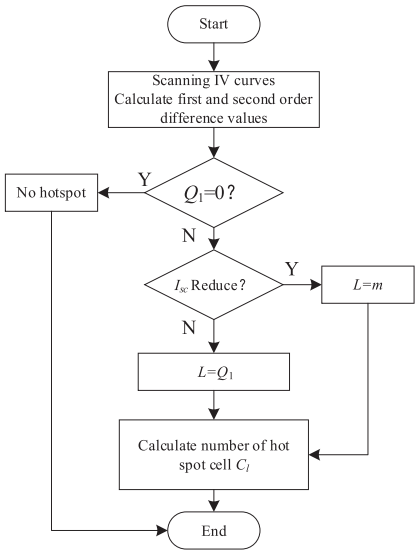

Fig. 5. Flowchart for PV module hot spot status identification.

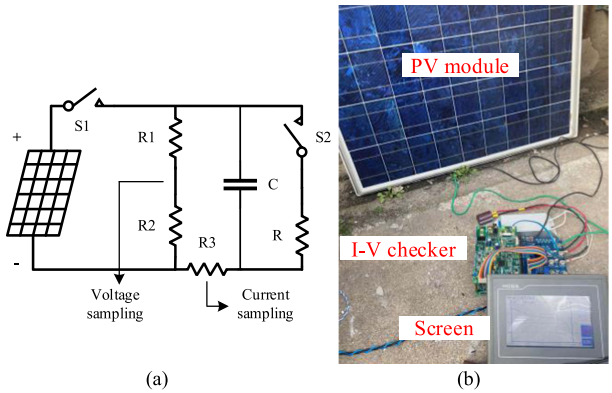

Fig. 6. Testbed for PV module *I–V* scanning. (a) *I–V* checker circuit. (b) Experimental platform.

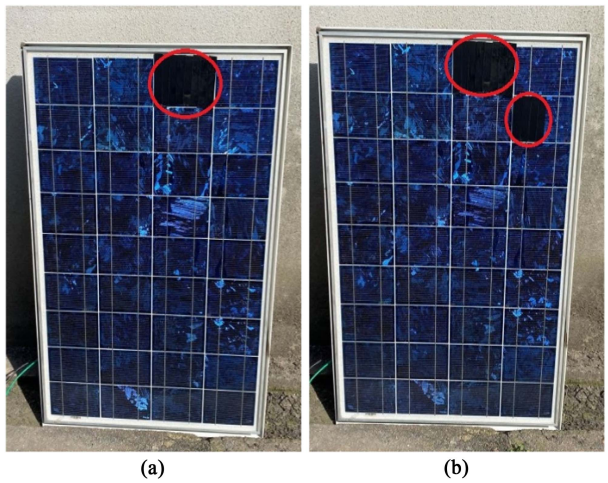

Fig. 7. PV module state. (a) One hotspot cell. (b) Two hotspot cells.

Specifically, if an assembly contains m strings and each string contains n cells, the number of strings containing hotspot cells is $L(0 \leq L \leq m)$. When $L \neq 0$, let the number of hotspot cells contained in the Lth cell string be $C_1, C_2, \cdots C_l \cdots, C_L(1 \leq C_l \leq n)$. Let the PV module *I–V* curve correspond to a second-order difference curve with Q1 positive outliers. The above first-order difference image and Fig. 2(a) show that if the short-circuit current value in the PV module *I–V* scan curve decreases, all m strings contain hotspot faults, with $L = m$. However, if the short-circuit current in the PV module *I–V* scan curve remains constant and the first-order difference curve has nonconducting points, the PV module contains a hotspot fault, $L = Q_1$. Moreover, if the short-circuit current in the PV module *I–V* scan curve does not decrease and the first-order difference curve is smooth and has no nonconducting points, the PV module contains no hotspot faults, $L = Q_1 = 0$. Furthermore, for any PV module with hotspot failure, the number of hotspot cells per string must be determined. The coordinate axis contains positive outliers, and the number of negative outliers in each area is increased by one and is thus equal to the number of hotspot cells in each string. Taking Fig. 4(b) as an example, the number of negative outliers in the coordinate axis intervals 0∼PT1 and PT1∼PT2 is 0 and 1 (i.e., PT_3 in Fig. 4), so the number of hotspot cells in the two hotspot strings are 1 and 2, respectively, that is, $C_1 = 1, C_2 = 2$.

In summary, the flowchart for PV module hotspot status identification is as follows:

In addition, our research group built a test platform to validate the PV module *I–V* checker, as shown in Fig. 6, where C = 680μF ,$R_1 = 10\Omega$, $R_2 = 110\Omega$,$R_3 = 1\Omega$, and $R = 588\Omega$. At the beginning of the test, S_2 is closed and S_1 is disconnected. Then, capacitor C is discharged through discharge resistor R so that the initial value of the capacitor voltage is 0 V. Then, S_2 is disconnected and S_1 is closed so that the PV module charges capacitor C. The voltage across the capacitor is sampled by voltage dividers R_1 and R_2, and the current flowing through the capacitor is sampled by shunt R_3. Initially, the charging circuit has zero impedance, and the PV module short-circuit current can be acquired. After approximately 50 ms, the capacitor is fully charged, and the open-circuit voltage of the PV module is measured. The sampled voltage and current (1000 data points each) are used to display the *I–V* curve on the LCD screen.

We cover different areas of the PV cells in our experiments to simulate hotspot failures with different severities. The experimental PV module state diagrams and *I–V* scan test results are shown below. Figs. 7 and 8 show that the *I–V* curve variation in the hotspot PV module during the experiment is consistent with the theoretical analysis.

The *I–V* scan curve data contain noise due to the accuracy of the sensor. We investigated the performance of the algorithm under high-frequency noise interference, as shown in Fig. 9. The PV module *I–V* scan curve with a noisy signal is shown in Fig. 9(a), and its first-order differential K and second-order differential K_2 are calculated and shown in Fig. 9(b) and (c), respectively.

Calculation errors due to the high-frequency noise can be observed when calculating K and K_2. However, the first quadrant of Fig. 9(c) shows that the change caused by this noise error is considerably smaller than the eigenvalue of the hotspot fault; thus, this effect can be eliminated by setting a suitable threshold interval. In some special cases, such as when a string contains

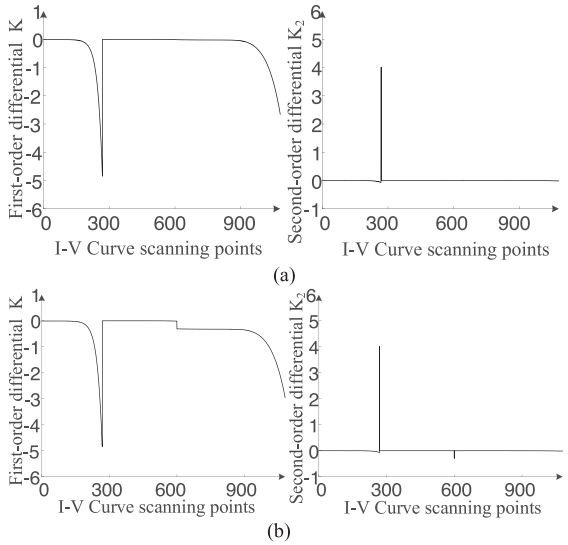

Fig. 8. *I–V* scan results. (a) One hotspot cell. (b) Two hotspot cells.

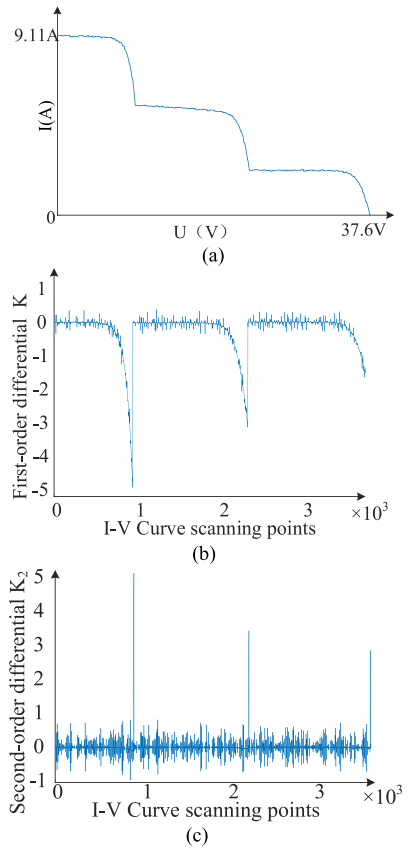

Fig. 9. *I–V* scans with noise. (a) *I–V* scan curve with a noisy signal. (b) K value under the influence of noise. (c) K_2 values under the influence of noise.

multiple hotspot cells, noise errors can cause issues. However, since *I–V* scanning circuits typically contain *RC* filtering links, high-frequency noise can be removed by filtering the hardware circuit, thus ensuring that noise does not affect the analyses of K and K_2.

III. Temperature Model

After the characteristics of the PV module were determined in various hotspot states, a temperature model was developed to estimate the normal individual temperature, T_w and the hotspot cell temperatureT_f in the PV module.

A. Principle of the PV Module Temperature Inverse Solution Model

For PV modules, the most basic physically resolved expression is

$$I = I_L - I_0\left\{\exp\left[\frac{q(V+IR_s)}{\mathrm{A_1KT}}\right]-1\right\}-\frac{V+IR_s}{R_{sh}} \quad (1)$$

whereI_L is the photocurrent,I_0 is the reverse saturation current,q is the electron charge, K is the Boltzmann constant, T is the absolute temperature, $\mathrm{A_1}$ is the diode factor, R_s is the series resistance, and R_{sh} is the parallel resistance. While this equation has been widely used in theoretical analyses of PV modules, it cannot be used to directly evaluate the temperature because the parameters I_L , I_0, $\mathrm{A_1}$, $R_s$and R_{sh} in this expression are not only related to the cell temperature and solar intensity but are also difficult to determine in practice. Because the actual factory parameters of PV modules usually include the open-circuit voltage U_{oc}, short-circuit current I_{sc}, maximum power point voltage U_m, current I_m, and power P_m under standard test conditions (STC), the temperature estimation model should include these available module parameters in practice. In addition, since the module temperature estimation ultimately needs to obtain specific temperature values, the model should contain an explicit expression of the module temperature without transcendental functions. Considering the above requirements, this article uses the engineering PV module model shown in (2), which includes parameters such as the open-circuit voltage, short-circuit current, and ambient temperature, as the base model for estimating the module temperature. If the voltage at the end of the PV module is set to U and the output current is set to I, the following engineering relationship exists [15]:

$$I = I_{sc}^*\left[1-C_1^*\left(\exp\left(\frac{U}{C_2^*\cdot U_{oc}^*}\right)-1\right)\right] \quad (2)$$

where C_1^*, C_2^* are coefficients; U_{oc}^* is the corrected open-circuit voltage; and I_{sc}^* is the corrected short-circuit current. The coefficients C_1^*, C_2^* are determined using

$$\begin{cases} C_1^* = \left(1-\frac{I_m^*}{I_{sc}^*}\right)\exp\left(-\frac{U_m^*}{C_2^*U_{oc}^*}\right) \\ C_2^* = \frac{U_m^*/U_{oc}^*-1}{\ln\left(1-\frac{I_m^*}{I_{sc}^*}\right)} \end{cases} \quad (3)$$

where U_m^* is the corrected maximum power point voltage and I_m^* is the corrected maximum power point current. The parameters $U_m^*, I_m^*, U_{oc}^*, I_{sc}^*$ are determined using

$$\begin{cases} I_{sc}^* = I_{sc}\Delta I \\ I_m^* = I_m\Delta I \\ U_{oc}^* = U_{oc}\Delta U \\ U_m^* = U_m\Delta U \end{cases} \quad (4)$$

where U_{oc} is the open-circuit voltage under standard test conditions (STC); I_{sc} is the short-circuit current under STC; U_m is the maximum power point voltage under STC; I_m is the maximum power point current under STC; ΔU is a voltage correction parameter; and ΔI is a current correction parameter. The values of ΔU and ΔI are determined using

$$\begin{cases} \Delta I = \frac{S}{S_{ref}}\left[1 + a\left(T - T_{ref}\right)\right] \\ \Delta U = \left[1 - c\left(T - T_{ref}\right)\right]\ln\left[e + b\left(S - S_{ref}\right)\right] \end{cases} \tag{5}$$

where a, b, c are constant factors whose values can be set to $a = 0.0025, b = 0.0005$,and $c = 0.00288$, respectively, according to the typical values given in the literature [15]. Previous works have shown [15] that the model error of the PV module does not exceed 6% under these parameter settings. The coefficient e is a natural constant with a value of approximately 2.71828. S_{ref} is the standard irradiance and is taken as 1000 W/m^2; T_{ref} is the standard module temperature and is taken as 25 °C; S is the actual irradiance of the environment; and T is the actual temperature of the module.

In summary, (2) provides an explicit relational model for the *I–V* characteristics of a PV module. After the factory STC parameters U_{oc} , I_{sc}, U_m, and I_m are determined, the output current of the module can be uniquely determined by measuring the actual irradiation S and temperature T of any module operating in the studied environment. Moreover, for a given module, the actual temperature of the module can be determined based on the collected module output power at the maximum power point tracker (MPPT) and the ambient irradiation. This is the basic principle of the inverse solution model of the module temperature.

B. Normal PV Cell Temperature Estimation

Based on the above inverse solution principle, the solution model used to obtain the module temperature can be described as follows. Since the module power is adjusted by the MPPT controller, the operating point of the actual module is always located at the maximum power point in the I–*V* characteristic curve, which is determined by the module temperature and irradiation. Assuming that the module does not fail, at a certain irradiation S and module temperature T, the following equation exists:

$$\begin{aligned} P_m^* &= U_m^* \cdot I_m^* = U_m \Delta U \cdot I_m \Delta I \\ &= U_m I_m \cdot \Delta U \Delta I = P_m \cdot \Delta U \Delta I \end{aligned} \tag{6}$$

where P_m^* is the current maximum power of the module and P_m is the maximum power under STC. Thus, we can obtain the following equation:

$$\frac{P_m^*}{P_m} = \Delta U \Delta I \tag{7}$$

Substituting this equation into (5) yields the following formula:

$$AT^2 + BT + C = \frac{P_m^*}{P_m} \tag{8}$$

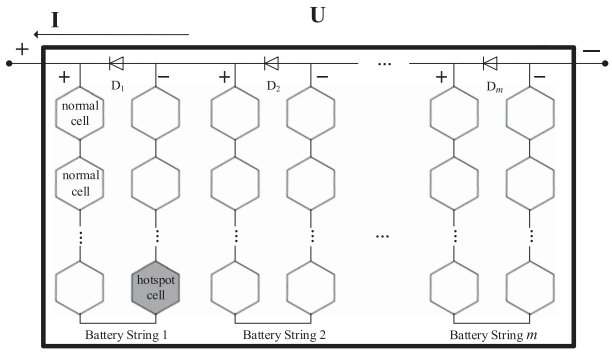

Fig. 10. Status diagram of a single-cell hotspot model.

$$\text{where} \begin{cases} A = -\frac{acS\ln(e+b(S-S_{ref}))}{S_{ref}} \\ B = \frac{(a-c+2acT_{ref})S\ln(e+b(S-S_{ref}))}{S_{ref}} \\ C = \frac{\left(1-aT_{ref}-acT_{ref}^2+cT_{ref}\right)S\ln(e+b(S-S_{ref}))}{S_{ref}} \end{cases}$$

Equation (8) indicates that for some PV module, S_{ref}, T_{ref}, P_m parameters are known, the actual output power (P_m^*) and actual irradiation (S) can be measured, and the PV module temperature (T) can be determined by solving the above equation. For PV modules with hotspots, the temperatures of the normal internal cells usually do not change extensively before or after the PV module generates a hotspot; thus, the temperatures of all normal cells in the PV module are assumed to be equal to the temperature of the PV module in the temperature estimation.

C. Hotspot Cell Temperature Estimation

In practice, module temperature abnormalities appear as high temperatures in some cells in the module. The model in the previous section determines the temperature T_w of all normal PV cells in a module. For a hotspot cell in a module, the temperature should be estimated based on the characteristics of the hotspot state of the module. Take the structure shown in Fig. 1 as an example and consider a hotspot with a fault described by $L = 1, C_1 = 1$ at a certain moment. The state of each cell in such a module is shown in Fig. 10, where the temperature of the normal cell is estimated as T_w and the temperature of the only hotspot cell is recorded as T_{f1}.

As shown in Fig. 10, because bypass diode D_1 is located within the string containing the hotspot cell, this string does not produce power externally; instead, the output power of all normal cells in the string is consumed by the faulty cell as thermal energy, leading to high temperatures in the faulty cell region. The corresponding heat balance model is shown in Fig. 11.

Fig. 11 shows that, from a heat balance perspective, the power associated with the hotspot cell temperature should satisfy

$$P_{get} = P_{loss}, \text{where} \begin{cases} P_{get} = P_{radin} + P_{sun} + P_e \\ P_{loss} = P_{con} + P_{wind} + P_{radout} \end{cases} \tag{9}$$

where P_{get}, P_{loss} represent the total absorbed and dissipated power, respectively; P_{radin} denotes the input power due to

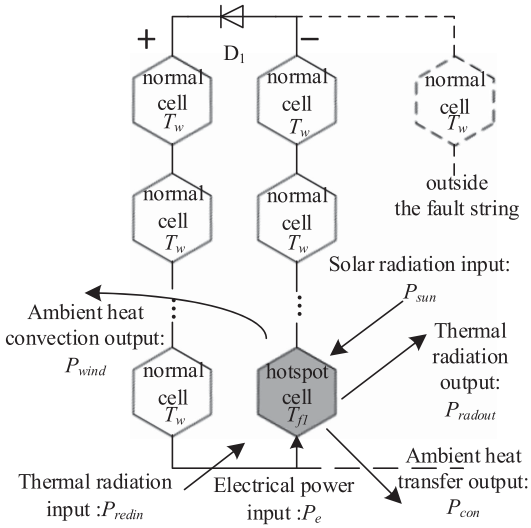

Fig. 11. Heat balance model of a failed cell.

thermal radiation; P_{sun} is the power due to solar radiation; P_e is the sum of the normal power in the faulty string; P_{con} is the ambient heat transfer power; P_{wind} is the air thermal convection power; and P_{radout} is the thermal radiation input power. Since the faulty cell is in the shaded state, its irradiance is usually significantly reduced and maintained at a low level that can be approximated as its power:$P_{sun} \approx 0$, P_e. According to the *I–V* characteristics of the string solution described in Section II-A, a power estimation formula for heat dissipation [16] that considers the effects of windward- and leeward-oriented PV modules and varying ambient temperatures has been developed. These factors can also be considered simultaneously, as follows:

$$\begin{cases} P_{con} + P_{wind} = \eta A(T_{f1} - T_c) \\ \eta = (17.1 + 5.7v) \end{cases} \tag{10}$$

where η is the thermal energy conversion factor. A previous report [17] noted that for PV modules, η can be considered a constant and taken as $\eta = 28.8\mathrm{W}^{\circ}\mathrm{C}^{-1}\mathrm{m}^{-2}$. However, if wind speed variations are considered, the calculated η value is more accurate, significantly improving the estimated energy dissipation. Thus, to improve the accuracy of the analysis, this article considers the effect of wind speed. In practice, such as when the accuracy of the temperature assessment is less important, wind speed variations can be ignored to reduce the complexity of the model.A is the upper surface area of the cell (m^2); T_c is the ambient temperature; and v is the ambient wind speed on the windward side (m/s). Finally, P_{radin} and P_{radout} values can be determined according to the Stefan–Boltzmann law [18] with the following equations:

$$\begin{cases} P_{radin} = 2A\sigma(T_c + 273)^4 \\ P_{radout} = 2A\sigma(T_{f1} + 273)^4 \\ \sigma = {2\pi^5\mathrm{k}^4}/{15\mathrm{h}^3\mathrm{c}^2} = 5.67 \times 10^{-8}\mathrm{W}/\left(\mathrm{m}^2 \cdot K^4\right) \end{cases} \tag{11}$$

where σ is a constant coefficient and h, c, and k are Planck's constant, the speed of light in a vacuum, and Boltzmann's constant, respectively. After the power relationship of each PV module has been determined, as the faulty cell continues to heat up until the temperature stabilizes, the power relationship can be iterated based on the power balance condition until the temperature equilibrium point has been reached and T_{f1} has been obtained. The specific temperature estimation process for cell-level PV modules is summarized in Fig. 12.

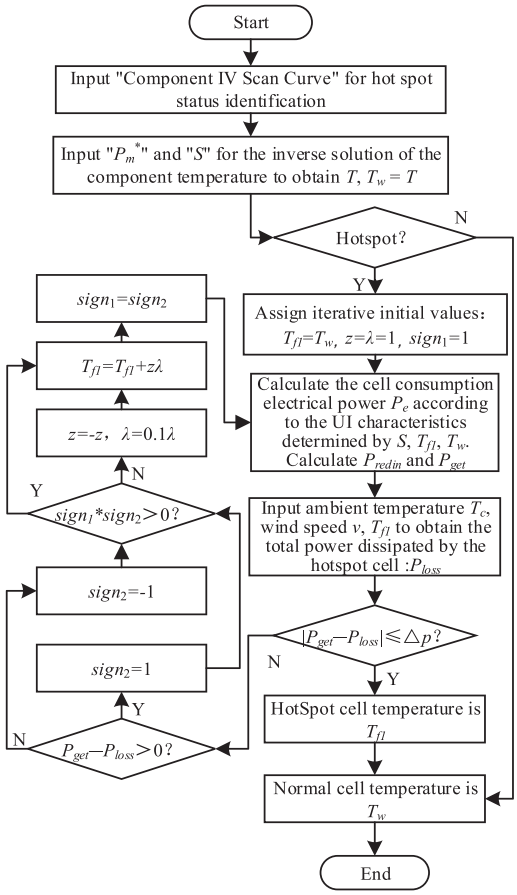

Fig. 12. Flowchart of the PV module temperature estimation model.

In the figure, Δp is the given nonnegative iteration accuracy, λ is the iteration step, z is the one-dimensional iteration direction, and signs 1 and 2 record the sign of the power difference twice to determine the correct iteration direction. The initial temperature of the hotspot cell should be equal to the temperature of the normal cell immediately before the PV module generates a hotspot and begins to warm up; thus, the algorithm sets the initial temperature of the hotspot cell to T_w. In addition, the iterative algorithm reverses the iteration direction z each time the power difference value changes its sign and reduces the number of iterations to ensure that the algorithm converges to the required iteration accuracy. Thus, the final temperature of the hotspot cell is estimated, and the temperature range of the cell in the module can be obtained by combining the hotspot cell temperature and the estimated temperature of the normal PV cells, achieving a cell-level module temperature estimation.

IV. Experimental Validation

The temperature estimation algorithm is validated with actual data collected at a PV power plant in Badong, Hubei. The module

TABLE II
PV MODULE PARAMETER TABLE

Parameter	Value
Open-circuit voltage (U_{oc})	38.1 V
Short-circuit current (I_{sc})	9.32 A
STC maximum power point voltage (U_m)	31.1 V
STC maximum power point curve (I_m)	8.84 A
STC irradiation (S_{ref})	1000 W/m^2
STC temperature (T_{ref})	25 °C
Number of module cell strings (m)	3
Number of single-string cells (n)	20
Single cell area (A)	2.73×10^{-2} m^2

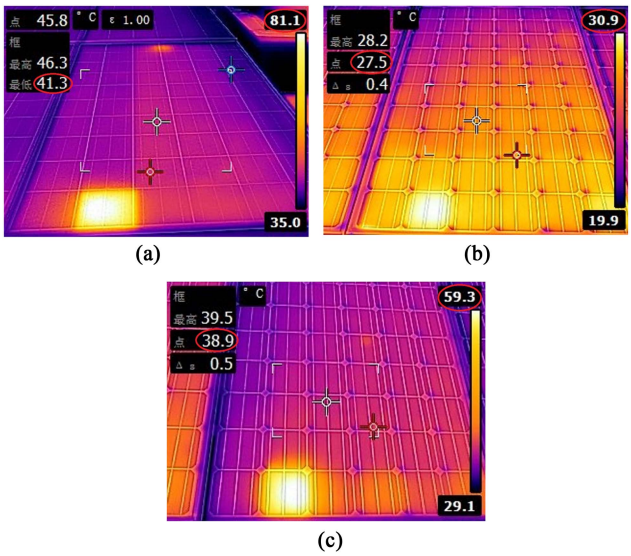

Fig. 13. Infrared images of PV module hotspots. (a) Case 1. (b) Case 2. (c) Case 3.

TABLE III
PV MODULE WORKING CONDITIONS

Case	Date	S (W/m^2)	T_c (°C)	V (m/s)	P_m^* (W)
1	6–10; 10:05	681	35.1	0.3	174.5
2	7–2; 19:25	385	19.9	0.6	93
3	7–21; 8:18	515	29.1	0.1	127

model used in this power plant is TSM-265PD05 from Trina Solar, and the module parameters are shown in Table II.

Three infrared images of PV module hotspot diagnoses collected by the power plant cloud platform in summer 2021 are shown in Fig. 13, and their corresponding environmental parameters are shown in Table III.

Fig. 13 shows that all three hotspot cases included single-string hotspot failures, with all strings containing only one faulty cell. To fully verify the accuracy of the temperature estimation algorithm for both normal and hotspot PV modules, hotspot PV module instances and normal PV module instances should both

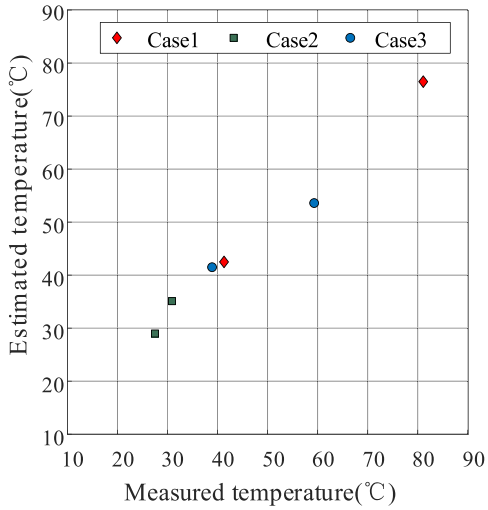

Fig. 14. Graph of PV module temperature estimation results.

TABLE IV
PV MODULE TEMPERATURE ESTIMATION RESULTS

Case	Estimated temp. (°C)	Actual temp. (°C)	Low temp. error	High temp. error	Average error
1	42.5~76.5	41.3~81.1	2.9%	5.7%	4.3%
2	29.0~35.1	27.5~30.9	5.4%	13.5%	9.45%
3	41.5~53.6	38.9~59.3	6.7%	9.6%	8.15%

be considered; however, due to the bypass diodes, the hotspot states of different strings in the PV module are relatively independent. Thus, when the maximum and minimum temperatures of a hotspot PV module are estimated, the temperatures of the string with the hotspot fault and a normal string can be estimated simultaneously. Therefore, the minimum and maximum temperature estimation errors of the PV module reflect the accuracy of the temperature estimation algorithm for the hotspot and normal PV modules, respectively.

By setting the iterative accuracy to $\Delta p = 0.1$, the temperatures of the faulty and normal cells in each assemblage can be estimated using the above algorithm and compared with the IR image data; the results are shown in Fig. 14 and Table IV.

Modules contain several PV cells, especially hotspot modules, and the temperatures of these PV cells vary. Therefore, in terms of the actual temperature of the module, the estimated temperature shown in Fig. 14 is a temperature range with considerable variation, where the highest and lowest temperatures are determined by the highest and lowest PV cells in the module, respectively. Thus, the module temperature range observed in the infrared image can be compared with the algorithm result to verify the effectiveness of the algorithm in evaluating the temperatures of normal and hotspot PV cells.

Fig. 14 shows that while the temperature estimation results obtained using the proposed algorithm are similar to the temperatures in the infrared images, certain errors still exist in the overall results. For the lower limit temperature data, the estimated results are influenced by the measured power P_m^*; however, due to the lack of an I–V curve-scanning function for

the power station, as no module optimizer has been installed, the measured power of the individual modules in the station can be estimated only by the dc power input on the inverter side, possibly leading to errors in the temperature estimations. The upper-limit temperature data are not only influenced by the current environmental state of the PV module but are also related to the historical PV module states, and the algorithm for estimating the upper-limit temperatures depends on the PV module remaining in its current state until thermal equilibrium is reached. However, because the maximum temperature of the faulty cell is estimated without considering the historical state or sudden changes in the environmental conditions of the PV module, the algorithm cannot match the real-time infrared data completely, resulting in errors in the results. Additionally, the irradiance level has a small effect on the temperature calculation error when the minimum temperature of the PV module is calculated using the inverse solution model. However, Tables III and IV show that when the maximum temperature of the PV module is calculated using the thermal equilibrium model, the error in the calculated PV module temperature increases gradually as the irradiance level increases because the electric-thermal power reaches equilibrium at a higher value under high irradiance conditions when the absolute power estimation error increases, which indirectly increases the temperature estimation error.

V. Conclusion

In this work, the characteristic parameters of PV modules are used to identify PV module hotspots based on the morphological characteristics of the PV module *I–V* scanning curve. Then, an inverse solution model is established to estimate the normal PV module temperature according to these characteristics. By combining this inverse model with the heat balance model of a faulty cell, the temperature of the faulty cell can be estimated, thus providing the overall distribution of the PV module temperature. Finally, infrared data acquired at a power station in Badong, Hubei, are used to verify the algorithm, and the results support the following conclusions:

1) The inverse solution of the normal module temperature can be determined based on the module characteristics, and the estimated temperatures are close to the actual temperatures. The estimation error of the inverse solution model can be reduced to a certain extent by improving the monitoring accuracy of the module power output by installing module optimizers and applying *I–V* scan functions.
2) Based on the thermal equilibrium model of a faulty cell, the theoretical final temperature of a hotspot cell can be estimated by treating the working and environmental states of the PV module as constants until thermal equilibrium is reached. In practice, the PV module and the environmental state can change in real time; thus, some errors arise between the theoretical final temperature and the maximum temperature of the PV module. However, the algorithm can estimate the temperature range of a PV module more accurately than previous methods, and the proposed algorithm has a high reference value for generating fire warnings associated with PV modules.

In terms of cost, most PV plants are already equipped with environmental monitors for irradiance measurements, regardless of whether they are equipped with module temperature monitoring systems. Therefore, to apply the method proposed in this article, power stations do not need to purchase additional irradiation measurement instruments. Compared with the additional economic investment of using temperature sensors or infrared imagers for temperature estimations, the proposed method is a more economical choice.

References

[1] Hoeven Mvd. *Technology Roadmap: SOlar Photovoltaic Energy [R]*. Paris: International Energy Agency's Renewable Energy Division, 2014.
[2] S. Vergura, "Correct settings of a joint unmanned aerial vehicle and infrared camera system for the detection of faulty photovoltaic modules," *IEEE J. Photovolt.*, vol. 11, no. 1, pp. 124–130, Jan. 2021.
[3] Y. Su, F. Tao, J. Jin, and C. Zhang, "Automated overheated region object detection of photovoltaic module with thermography image," *IEEE J. Photovolt.*, vol. 11, no. 2, pp. 535–544, Mar. 2021.
[4] E. Roibás-Millán et al., "Lambert W-function simplified expressions for photovoltaic current-voltage modelling," in *Proc. IEEE Int. Conf. Environ. Elect. Eng. IEEE Ind. Commercial Power Syst. Europe*, 2020, pp. 1–6.
[5] M. Prilliman, J. S. Stein, D. Riley, and G. Tamizhmani, "Transient weighted moving-average model of photovoltaic module back-surface temperature," *IEEE J. Photovolt.*, vol. 10, no. 4, pp. 1053–1060, Jul. 2020.
[6] J. Oh et al., "Reduction of PV module temperature using thermally conductive backsheets," *IEEE J. Photovolt.*, vol. 8, no. 5, pp. 1160–1167, Sep. 2018.
[7] C. Li, S. V. Spataru, K. Zhang, Y. Yang, and H. Wei, "A multi-state dynamic thermal model for accurate photovoltaic cell temperature estimation," *IEEE J. Photovolt.*, vol. 10, no. 5, pp. 1465–1473, Sep. 2020.
[8] W. Gao and R. -J. Wai, "A novel fault identification method for photovoltaic array via convolutional neural network and residual gated recurrent unit," *IEEE Access*, vol. 8, pp. 159493–159510, 2020, doi: 10.1109/ACCESS.2020.3020296.
[9] H. P. -C. Hwang, C. C. -Y. Ku, and J. C. -C. Chan, "Detection of malfunctioning photovoltaic modules based on machine learning algorithms," *IEEE Access*, vol. 9, pp. 37210–37219, 2021.
[10] C. F. Abe, J. B. Dias, G. Notton, and P. Poggi, "Computing solar irradiance and average temperature of photovoltaic modules from the maximum power point coordinates," *IEEE J. Photovolt.*, vol. 10, no. 2, pp. 655–663, Mar. 2020.
[11] Y. Hishikawa et al., "Translation of solar cell performance for irradiance and temperature from a single I-V curve without advance information of translation parameters," *IEEE J. Photovolt.*, vol. 9, no. 5, pp. 1195–1201, Sep. 2019.
[12] M. Muñoz Escribano et al., "Module temperature dispersion within a large PV array: Observations at the amareleja PV plant," *IEEE J. Photovolt.*, vol. 8, no. 6, pp. 1725–1731, Nov. 2018.
[13] Z. Zhixiang, "Research on fault diagnosis method of crystalline silicon photovoltaic module based on I–V characteristic analysis," Master's thesis, Hefei University of Technology, (in chinese), Nov. 2020.
[14] L. Heng, "Comprehensive research on fault diagnosis and condition evaluation of hot spot photovoltaic modules based on I-V curve," Master's thesis, Hefei University of Technology, (in chinese), Nov. 2020.
[15] S. Jianhui and Y. Shijie, "Mathematical model for silicon solar cell engineering," (in chinese) *J. Sol. Energy*, vol. 22, no. 4, pp. 409–412, Nov. 2001.
[16] C. Ze, Y. Genyuan, and L. Li, "Estimation of photovoltaic module temperature based on energy conservation," (in chinese) *J. Sol. energy*, vol. 39, no. 7, pp. 1875–1884, Jul. 2018.
[17] M. Mattei et al., "Calculation of the polycrystalline PV module temperature using a simple method of energy balance[J]," *Renewable Energy*, vol. 31, no. 4, pp. 553–567, 2006.
[18] W. Bin, "Research on thermal radiation temperature measurement technology," Master's thesis, Harbin Engineering University, (in chinese), Nov. 2012.